J. Shanghai Jiaotong Univ. (Sci.), 2016, 21(4): 385-394
DOI: 10.1007/s12204-016-1737-9

Dynamic Modeling and Active Control of a Strap-on Launch Vehicle

LIU Pan (刘　盼), *GUO Shaojing* (郭绍静), *CAI Guoping** (蔡国平)
(Department of Engineering Mechanics; State Key Laboratory of Ocean Engineering, Shanghai Jiaotong University, Shanghai 200240, China)

Abstract: Dynamic modeling and active control of a strap-on launch vehicle are studied in this paper. In the dynamic modeling, the double-compatible free-interface modal synthesis method is used to establish dynamic model of the system, and its model precision is compared with those of finite element method (FEM), fixed-interface modal synthesis method and free-interface modal synthesis method. In the active control, the swing angle of rocket motor is used as design variable, and the control law design based on the model of mass center motion is adopted to validate the system. Simulation results indicate that the double-compatible model synthesis method can properly approximate the FEM which is used as the benchmark solution, and the model precision of the double-compatible modal synthesis method is obviously higher than those of the fixed-interface and free-interface modal synthesis methods. Based on the control law design, the deflection of mass center of the launch vehicle is very small.
Key words: strap-on launch vehicle, dynamic modeling, active control
CLC number: V 414.1　　**Document code:** A

0 Introduction

It is well known that flexible components are vastly used in aerospace structures due to the limit on the weight of launch vehicle. In order to deliver more payloads to outer space, launch vehicle trends to long thruster so as to carry more fuel. This results in obvious flexibility of the launch vehicle. The introduction of flexibility brings big difficulty to dynamic modeling and control system. To exactly describe dynamic behavior of the system, researcher should adequately take the flexible characteristics in the system into account to establish the very high order of dynamic model in the modeling process. But control design and implement require that the order of the system should be as low as possible. Therefore, model reduction work should be done so as to obtain a low-order mode convenient for control design. This low-order mode should be able to reflect the dynamic characteristics of the original system and its order should be low enough too. On the other hand, from the point of dynamic simulation, model order should not be high so as to improve computational efficiency.

For linear structure, lower-order modes play a main role in dynamic response of the structure. So the lower-order modes are often preserved to form a reduction model to represent the original system approximately. This is the so-called modal truncation technique which has been widely applied to both theoretical research and engineering application. Essentially, the modal synthesis technique using the modal truncation technique is a method to build low-order dynamic model for complex system. In the modal synthesis method, the complex system is divided into several components reasonably, and high-order dynamic equation of each component is firstly established by finite element method (FEM). Then, the modal truncation technique is applied to the FEM equation to obtain a low-order modal dynamic equation of the component. Finally, the dynamic equation of the system is established by doing the modal synthesis for all the components based on displacement and force compatibility conditions at interfaces of the components. Up to now, some different types of modal synthesis methods have been proposed by researchers according to different selection of modal function of flexible component[1-4]. The typical ones are the free-interface modal synthesis method and the fixed-interface modal synthesis method. In Refs. [4-5], the free-interface modal synthesis method is modified, a double-compatible free-interface modal synthesis method is proposed, and this method can

Received date: 2014-10-31
Foundation item: the National Natural Science Foundation of China (Nos. 11132001, 11272202 and 11472171), the Key Scientific Project of Shanghai Municipal Education Commission (No. 14ZZ021), and the Natural Science Foundation of Shanghai (No. 14ZR1421000)
∗**E-mail:** caigp@sjtu.edu.cn

achieve higher computational precision than the free-interface and fixed-interface modal synthesis methods. The modal synthesis method is applicable to dynamic modeling of large and complex engineering structures, and its validity has been justified in many practical applications[6-13]. For modern large-scale aerospace structure, the modal synthesis method is still an important and effective analysis tool. For example, space station is mainly composed of several cabins which are sent into space at different time. Generally, ground test needs to be done for every cabin before sending them into space. However, the overall ground test of space station is usually impossible. For this case, the modal synthesis method is available to get the characteristics of the space station by synthesizing data of every cabin.

All flight vehicles require manipulation (i.e., adjustment or control) of position, velocity and attitude (or orientation) for successful and efficient flight. A spacecraft launch rocket must achieve the necessary orbital velocity while it maintains a particular plane of flight. A missile rocket has to track a maneuvering target such that an intercept is achieved before running out of propellant. An atmospheric entry vehicle must land at a particular point with a specific terminal energy without exceeding the aero-thermal load limits. In all of these cases, precise control of the vehicle attitude is required all the time since the aerodynamic forces governing an atmospheric trajectory are very sensitive to the body's orientation relative to the flight direction. Furthermore, in some cases attitude control alone is crucial for the mission success. Therefore, attitude dynamics analysis is necessarily complex due to these factors mentioned above. For example, Explorer 1 as the first U.S. satellite in February 1958 is useless as an observation or communication platform due to tumbling, even though it may be in the desired orbit.

Any flight vehicle must have two separate classes of control systems: ① control of position and linear velocity relative to a planet fixed frame, called trajectory control; ② control of vehicle's orientation (attitude control) with respect to a frame of reference. Over the years, many scholars have dedicated to the study of the space vehicle attitude dynamics analysis and active control design[14-21]. A launch vehicle is essentially a long slender beam, and thus it is structurally very flexible. As a result, one significant risk for a large flexible launch vehicle ascent flight control system is the potential for interaction between the ascent flight control and the structural bending mode. The control system has the potential to excite the bending mode and destabilize the vehicle dynamics[22]. Since engines apply forces to the launch vehicle's structure, energy can be fed into the structure at various frequencies. This can reinforce elastic oscillations, ultimately leading to structural failure of the vehicle[23], or enlargement of deflection of mass centre of the vehicle.

In this paper, dynamic modeling and active control of a strap-on launch vehicle are investigated. The double-compatible modal synthesis method is used to establish the dynamic equation of the system, and the swing angle of motor thrust is used as a design variable to make the deflection of mass centre of the launch vehicle as small as possible. Simulation results prove the effectiveness of the theoretical analysis.

1 Dynamic Modeling by the Double-Compatible Free-Interface Modal Synthesis Method

1.1 Dynamic Equation

For a strap-on launch vehicle, the system may be described by beam model when the system is symmetrical and the vibration of the system is linear. As shown in Fig. 1(a), the launch vehicle is composed of a core stage and four boosters. Four boosters are identical and are symmetrically arranged with respect to the core stage. In this paper, the plane problem of the strap-on launch vehicle is considered, as shown in Fig. 1(b), where the core stage is represented by the long beam and the two boosters are represented by the short beams. The modal synthesis method is used to establish dynamic equation of the system. In the modal synthesis method, the system is divided into three substructures, as shown in Fig. 2. Substructures 1 and 3 are both connected to the long beam through two nodes shown as the big black dots in Fig. 2. In practice, it is expected that there only exists force action at the joint of the core stage and the boosters, where bending moment may cause deformation damage of the shell of the launch vehicle. So the joint of the long beam and the short beam in Fig. 2 can be regarded as the hinge joint. In other words, the interface force on the big black node in Fig. 2 only contains force component and does not contain bending moment. Three substructures in Fig. 2 are analyzed by

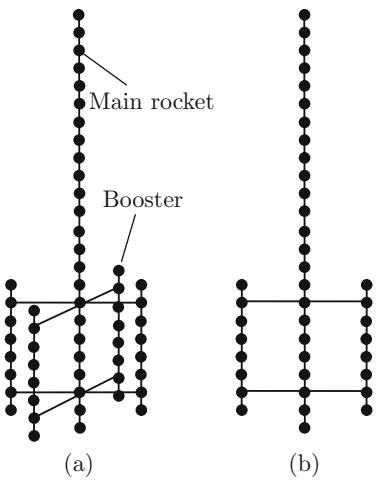

Fig. 1 Simplified model of strap-on launch vehicle

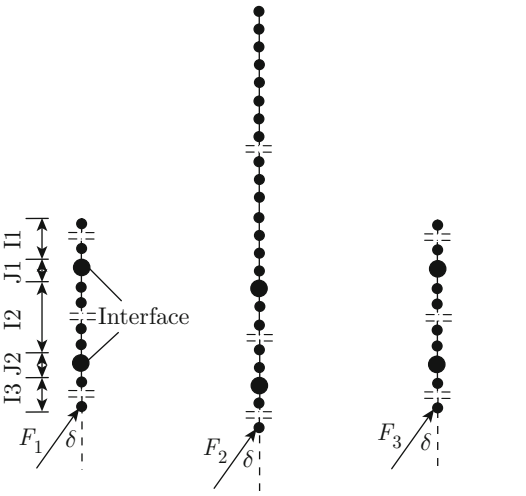

Fig. 2 Substructure division

FEM before the modal synthesis is done. The black dot in Fig. 2 represents the FEM node. Each dot has three degrees of freedom (DoFs), i.e. the transverse and axial displacements and the angle of cross-section. The parameters F_1, F_2 and F_3 are the thrusts produced by three engines of the core stage and the two boosters, they act at the lowest nodes of the three beams, as shown in Fig. 2, and the angles between the thrusts and the axial direction are all δ.

Substructure 1 is considered firstly in the FEM. It is divided into five sections: I1, J1, I2, J2 and I3, as shown in Fig. 2. The vectors of FEM node coordinates of these five sections are represented by $\boldsymbol{u}_{1\mathrm{I}1}$, $\boldsymbol{u}_{1\mathrm{J}1}$, $\boldsymbol{u}_{1\mathrm{I}2}$, $\boldsymbol{u}_{1\mathrm{J}2}$ and $\boldsymbol{u}_{1\mathrm{I}3}$, respectively, where $\boldsymbol{u}_{1\mathrm{I}1}$, $\boldsymbol{u}_{1\mathrm{I}2}$ and $\boldsymbol{u}_{1\mathrm{I}3}$ are the internal node coordinates, and $\boldsymbol{u}_{1\mathrm{J}1}$ and $\boldsymbol{u}_{1\mathrm{J}2}$ are the interface node coordinates. The first number "1" in subscript represents Substructure 1. For example, $\boldsymbol{u}_{1\mathrm{I}2}$ means the node-coordinate vector of the I2 section of Substructure 1. This kind of subscript expression will be used in this paper.

The FEM dynamic equation of Substructure 1 can be written as

$$\boldsymbol{M}_1\ddot{\boldsymbol{u}}_1 + \boldsymbol{K}_1\boldsymbol{u}_1 = \boldsymbol{B}_{1f}\boldsymbol{f}_{1\mathrm{J}} + \boldsymbol{B}_{1F}F_1. \tag{1}$$

In Eq. (1), $\boldsymbol{u}_1$ is the node-coordinate vector of Substructure 1, $\boldsymbol{u}_1 = [\boldsymbol{u}_{1\mathrm{I}1}^{\mathrm{T}} \ \boldsymbol{u}_{1\mathrm{J}1}^{\mathrm{T}} \ \boldsymbol{u}_{1\mathrm{I}2}^{\mathrm{T}} \ \boldsymbol{u}_{1\mathrm{J}2}^{\mathrm{T}} \ \boldsymbol{u}_{1\mathrm{I}3}^{\mathrm{T}}]^{\mathrm{T}}$; $\boldsymbol{M}_1$ and $\boldsymbol{K}_1$ are the mass and stiffness matrices, respectively; $\boldsymbol{f}_{1\mathrm{J}}$ is the interface-force vector of Substructure 1, $\boldsymbol{f}_{1\mathrm{J}} = [\boldsymbol{f}_{1\mathrm{J}1}^{\mathrm{T}} \ \boldsymbol{f}_{1\mathrm{J}2}^{\mathrm{T}}]^{\mathrm{T}}$, where $\boldsymbol{f}_{1\mathrm{J}1}$ and $\boldsymbol{f}_{1\mathrm{J}2}$ are the interface-force vectors of the two nodes of Substructure 1 connected to Substructure 2, respectively. Since there only exists force action on the two nodes, $\boldsymbol{f}_{1\mathrm{J}1}$ and $\boldsymbol{f}_{1\mathrm{J}2}$ both only contain the two force components in transverse and axial directions, respectively. The parameter $\boldsymbol{B}_{1f}$ is the Boolean indicated matrix of $\boldsymbol{f}_{1\mathrm{J}}$; F_1 is the external force of Substructure 1, namely the thrust of Substructure 1; $\boldsymbol{B}_{1F}$ is the Boolean indicated matrix of F_1. Since F_1 acts at the lowest node of the I3 section and the angle of inclination is δ, two elements of $\boldsymbol{B}_{1F}$ corresponding to F_1 are $\sin\delta$ and $\cos\delta$ with other elements of $\boldsymbol{B}_{1F}$ being zero.

The node-coordinate vector $\boldsymbol{u}_1$ can be rearranged as

$$\boldsymbol{u}_1^* = [\boldsymbol{u}_{1\mathrm{I}1}^{\mathrm{T}} \ \boldsymbol{u}_{1\mathrm{I}2}^{\mathrm{T}} \ \boldsymbol{u}_{1\mathrm{I}3}^{\mathrm{T}} \ \boldsymbol{u}_{1\mathrm{J}1}^{\mathrm{T}} \ \boldsymbol{u}_{1\mathrm{J}2}^{\mathrm{T}}]^{\mathrm{T}} = [\boldsymbol{u}_{1\mathrm{I}}^{\mathrm{T}} \ \boldsymbol{u}_{1\mathrm{J}}^{\mathrm{T}}]^{\mathrm{T}}, \tag{2}$$

where $\boldsymbol{u}_{1\mathrm{I}} = [\boldsymbol{u}_{1\mathrm{I}1}^{\mathrm{T}} \ \boldsymbol{u}_{1\mathrm{I}2}^{\mathrm{T}} \ \boldsymbol{u}_{1\mathrm{I}3}^{\mathrm{T}}]^{\mathrm{T}}$ and $\boldsymbol{u}_{1\mathrm{J}} = [\boldsymbol{u}_{1\mathrm{J}1}^{\mathrm{T}} \ \boldsymbol{u}_{1\mathrm{J}2}^{\mathrm{T}}]^{\mathrm{T}}$. The relationship between $\boldsymbol{u}_1$ and $\boldsymbol{u}_1^*$ is

$$\boldsymbol{u}_1^* = \boldsymbol{T}_1\boldsymbol{u}_1, \quad \boldsymbol{T}_1 = \begin{bmatrix} \boldsymbol{I} & \boldsymbol{0} & \boldsymbol{0} & \boldsymbol{0} & \boldsymbol{0} \\ \boldsymbol{0} & \boldsymbol{0} & \boldsymbol{I} & \boldsymbol{0} & \boldsymbol{0} \\ \boldsymbol{0} & \boldsymbol{0} & \boldsymbol{0} & \boldsymbol{0} & \boldsymbol{I} \\ \boldsymbol{0} & \boldsymbol{I} & \boldsymbol{0} & \boldsymbol{0} & \boldsymbol{0} \\ \boldsymbol{0} & \boldsymbol{0} & \boldsymbol{0} & \boldsymbol{I} & \boldsymbol{0} \end{bmatrix}, \tag{3}$$

where $\boldsymbol{I}$ is the identity matrix. Making transformation for Eq. (1) yields

$$\boldsymbol{M}_1^*\ddot{\boldsymbol{u}}_1^* + \boldsymbol{K}_1^*\boldsymbol{u}_1^* = \boldsymbol{B}_{1f}^*\boldsymbol{f}_{1\mathrm{J}} + \boldsymbol{B}_{1F}^*F_1, \tag{4}$$

where

$$\boldsymbol{M}_1^* = \boldsymbol{T}_1\boldsymbol{M}_1\boldsymbol{T}_1^{-1}, \quad \boldsymbol{K}_1^* = \boldsymbol{T}_1\boldsymbol{K}_1\boldsymbol{T}_1^{-1},$$
$$\boldsymbol{B}_{1f}^* = \boldsymbol{T}_1\boldsymbol{B}_{1f}, \quad \boldsymbol{B}_{1F}^* = \boldsymbol{T}_1\boldsymbol{B}_{1F}.$$

Making modal analysis for Substructure 1 yields

$$\boldsymbol{u}_1^* = \boldsymbol{\Phi}_{1n}\boldsymbol{p}_1 = [\boldsymbol{\Phi}_{1k} \ \ \boldsymbol{\Phi}_{1d}] \begin{bmatrix} \boldsymbol{p}_{1k}^{\mathrm{T}} \\ \boldsymbol{p}_{1d}^{\mathrm{T}} \end{bmatrix} = \boldsymbol{\Phi}_{1k}\boldsymbol{p}_{1k} + \boldsymbol{\Phi}_{1d}\boldsymbol{p}_{1d}, \tag{5}$$

where $\boldsymbol{\Phi}_{1n} = [\boldsymbol{\Phi}_{1k} \ \ \boldsymbol{\Phi}_{1d}]$ is the modal transformation matrix; $\boldsymbol{\Phi}_{1k}$ and $\boldsymbol{\Phi}_{1d}$ are the lower and higher modes of Substructure 1, respectively; $\boldsymbol{p}_1 = [\boldsymbol{p}_{1k}^{\mathrm{T}} \ \ \boldsymbol{p}_{1d}^{\mathrm{T}}]^{\mathrm{T}}$ is the modal coordinate vector of Substructure 1; $\boldsymbol{p}_{1k}$ and $\boldsymbol{p}_{1d}$ are the vectors corresponding to $\boldsymbol{\Phi}_{1k}$ and $\boldsymbol{\Phi}_{1d}$, respectively. Substituting Eq. (5) into Eq. (4) and left multiplying $\boldsymbol{\Phi}_{1n}^{\mathrm{T}}$, one can obtain

$$\tilde{\boldsymbol{M}}_1^*\ddot{\boldsymbol{p}}_1 + \tilde{\boldsymbol{K}}_1^*\boldsymbol{p}_1 = \tilde{\boldsymbol{B}}_{1f}^*\boldsymbol{f}_{1\mathrm{J}} + \tilde{\boldsymbol{B}}_{1F}^*F_1, \tag{6}$$

where

$$\tilde{\boldsymbol{M}}_1^* = \begin{bmatrix} \boldsymbol{\Phi}_{1k}^{\mathrm{T}}\boldsymbol{M}_1^*\boldsymbol{\Phi}_{1k} & \boldsymbol{\Phi}_{1k}^{\mathrm{T}}\boldsymbol{M}_1^*\boldsymbol{\Phi}_{1d} \\ \boldsymbol{\Phi}_{1k}\boldsymbol{M}_1^*\boldsymbol{\Phi}_{1d}^{\mathrm{T}} & \boldsymbol{\Phi}_{1d}^{\mathrm{T}}\boldsymbol{M}_1^*\boldsymbol{\Phi}_{1d} \end{bmatrix} = \begin{bmatrix} \tilde{\boldsymbol{M}}_{1k}^* & \boldsymbol{0} \\ \boldsymbol{0} & \tilde{\boldsymbol{M}}_{1d}^* \end{bmatrix},$$

$$\tilde{\boldsymbol{K}}_1^* = \begin{bmatrix} \boldsymbol{\Phi}_{1k}^{\mathrm{T}}\boldsymbol{K}_1^*\boldsymbol{\Phi}_{1k} & \boldsymbol{\Phi}_{1k}^{\mathrm{T}}\boldsymbol{K}_1^*\boldsymbol{\Phi}_{1d} \\ \boldsymbol{\Phi}_{1k}\boldsymbol{K}_1^*\boldsymbol{\Phi}_{1d}^{\mathrm{T}} & \boldsymbol{\Phi}_{1d}^{\mathrm{T}}\boldsymbol{K}_1^*\boldsymbol{\Phi}_{1d} \end{bmatrix} = \begin{bmatrix} \tilde{\boldsymbol{K}}_{1k}^* & \boldsymbol{0} \\ \boldsymbol{0} & \tilde{\boldsymbol{K}}_{1d}^* \end{bmatrix},$$

$$\tilde{\boldsymbol{B}}_{1f}^* = [\boldsymbol{\Phi}_{1k}^{\mathrm{T}} \ \ \boldsymbol{\Phi}_{1d}^{\mathrm{T}}]^{\mathrm{T}}\boldsymbol{B}_{1f}^*, \quad \tilde{\boldsymbol{B}}_{1F}^* = [\boldsymbol{\Phi}_{1k}^{\mathrm{T}} \ \ \boldsymbol{\Phi}_{1d}^{\mathrm{T}}]^{\mathrm{T}}\boldsymbol{B}_{1F}^*.$$

Writing Eq. (6) into the block matrix form yields

$$\tilde{\boldsymbol{M}}_{1k}^*\ddot{\boldsymbol{p}}_{1k} + \tilde{\boldsymbol{K}}_{1k}^*\boldsymbol{p}_{1k} = \boldsymbol{\Phi}_{1k}^{\mathrm{T}}\boldsymbol{B}_{1f}^*\boldsymbol{f}_{1\mathrm{J}} + \boldsymbol{\Phi}_{1k}^{\mathrm{T}}\boldsymbol{B}_{1F}^*F_1, \tag{7}$$

$$\tilde{\boldsymbol{M}}_{1d}^*\ddot{\boldsymbol{p}}_{1d} + \tilde{\boldsymbol{K}}_{1d}^*\boldsymbol{p}_{1d} = \boldsymbol{\Phi}_{1d}^{\mathrm{T}}\boldsymbol{B}_{1f}^*\boldsymbol{f}_{1\mathrm{J}} + \boldsymbol{\Phi}_{1d}^{\mathrm{T}}\boldsymbol{B}_{1F}^*F_1. \tag{8}$$

Equations (7) and (8) are the dynamic equations of low and high modes of Substructure 1, respectively. From Refs. [3-4], we know that the response of Substructure 1 is mainly dominated by Eq. (7) and the contribution of high modes to the response of Substructure 1 is close to the static part. If dynamic terms and external force in Eq. (8) are neglected, the static equation of Eq. (8) can be written as

$$\tilde{\boldsymbol{K}}_{1d}^{*}\boldsymbol{p}_{1d} \approx \boldsymbol{\Phi}_{1d}^{\mathrm{T}}\boldsymbol{B}_{1f}^{*}\boldsymbol{f}_{1\mathrm{J}}, \tag{9}$$

thus

$$\boldsymbol{p}_{1d} \approx \tilde{\boldsymbol{K}}_{1d}^{*-1}\boldsymbol{\Phi}_{1d}^{\mathrm{T}}\boldsymbol{B}_{1f}^{*}\boldsymbol{f}_{1\mathrm{J}}. \tag{10}$$

Substituting Eq. (10) into Eq. (5) yields

$$\begin{aligned}\boldsymbol{u}_{1}^{*} =& \boldsymbol{\Phi}_{1k}\boldsymbol{p}_{1k} + \boldsymbol{\Phi}_{1d}\tilde{\boldsymbol{K}}_{1d}^{*-1}\boldsymbol{\Phi}_{1d}^{\mathrm{T}}\boldsymbol{B}_{1f}^{*}\boldsymbol{f}_{1\mathrm{J}} = \\ & \boldsymbol{\Phi}_{1k}\boldsymbol{p}_{1k} + \boldsymbol{\Psi}_{1d}\boldsymbol{f}_{1\mathrm{J}},\end{aligned} \tag{11}$$

where $\boldsymbol{\Psi}_{1d} = \boldsymbol{\Phi}_{1d}\tilde{\boldsymbol{K}}_{1d}^{*-1}\boldsymbol{\Phi}_{1d}^{\mathrm{T}}\boldsymbol{B}_{1f}^{*}$ is actually the residual flexibility of the interface force $\boldsymbol{f}_{1\mathrm{J}}$, also called the residual mode[3-4], and it represents the static contribution of high modes. In the double-compatible free-interface modal synthesis method, $\boldsymbol{\Psi}_{1d}$ is used in modal synthesis for the system. However, in the classical free-interface modal synthesis method, only the low modes of Substructure 1 are used in modal synthesis and $\boldsymbol{\Psi}_{1d}$ is useless. In Subsection 1.2, it is demonstrated through numerical simulation that the use of $\boldsymbol{\Psi}_{1d}$ can greatly improve the accuracy of modal synthesis. Equation (11) shows that, as the modal coordinate $\boldsymbol{p}_{1k}$, the interface force $\boldsymbol{f}_{1\mathrm{J}}$ can also be regarded as a kind of modal coordinate.

Substituting Eq. (11) into Eq. (4) and left multiplying $[\boldsymbol{\Phi}_{1k}^{\mathrm{T}} \ \ \boldsymbol{\Psi}_{1d}^{\mathrm{T}}]^{\mathrm{T}}$, one can obtain

$$\bar{\boldsymbol{M}}_{1}^{*}\ddot{\bar{\boldsymbol{p}}}_{1} + \bar{\boldsymbol{K}}_{1}^{*}\bar{\boldsymbol{p}}_{1} = \bar{\boldsymbol{B}}_{1f}^{*}\boldsymbol{f}_{1\mathrm{J}} + \bar{\boldsymbol{B}}_{1F}^{*}F_{1}, \tag{12}$$

where

$$\bar{\boldsymbol{p}}_{1} = [\boldsymbol{p}_{1k}^{\mathrm{T}} \ \ \boldsymbol{f}_{1\mathrm{J}}^{\mathrm{T}}]^{\mathrm{T}},$$

$$\bar{\boldsymbol{M}}_{1}^{*} = \begin{bmatrix}\boldsymbol{\Phi}_{1k}^{\mathrm{T}}\boldsymbol{M}_{1}^{*}\boldsymbol{\Phi}_{1k} & \boldsymbol{\Phi}_{1k}^{\mathrm{T}}\boldsymbol{M}_{1}^{*}\boldsymbol{\Psi}_{1d} \\ \boldsymbol{\Phi}_{1k}\boldsymbol{M}_{1}^{*}\boldsymbol{\Psi}_{1d}^{\mathrm{T}} & \boldsymbol{\Psi}_{1d}^{\mathrm{T}}\boldsymbol{M}_{1}^{*}\boldsymbol{\Psi}_{1d}\end{bmatrix} = \begin{bmatrix}\bar{\boldsymbol{M}}_{1k}^{*} & \boldsymbol{0} \\ \boldsymbol{0} & \bar{\boldsymbol{M}}_{1d}^{*}\end{bmatrix},$$

$$\bar{\boldsymbol{K}}_{1}^{*} = \begin{bmatrix}\boldsymbol{\Phi}_{1k}^{\mathrm{T}}\boldsymbol{K}_{1}^{*}\boldsymbol{\Phi}_{1k} & \boldsymbol{\Phi}_{1k}^{\mathrm{T}}\boldsymbol{K}_{1}^{*}\boldsymbol{\Psi}_{1d} \\ \boldsymbol{\Phi}_{1k}\boldsymbol{K}_{1}^{*}\boldsymbol{\Psi}_{1d}^{\mathrm{T}} & \boldsymbol{\Psi}_{1d}^{\mathrm{T}}\boldsymbol{K}_{1}^{*}\boldsymbol{\Psi}_{1d}\end{bmatrix} = \begin{bmatrix}\bar{\boldsymbol{K}}_{1k}^{*} & \boldsymbol{0} \\ \boldsymbol{0} & \bar{\boldsymbol{K}}_{1d}^{*}\end{bmatrix},$$

$$\bar{\boldsymbol{B}}_{1f}^{*} = [\boldsymbol{\Phi}_{1k}^{\mathrm{T}} \ \ \boldsymbol{\Psi}_{1d}^{\mathrm{T}}]^{\mathrm{T}}\boldsymbol{B}_{1f}^{*}, \quad \bar{\boldsymbol{B}}_{1F}^{*} = [\boldsymbol{\Phi}_{1k}^{\mathrm{T}} \ \ \boldsymbol{\Psi}_{1d}^{\mathrm{T}}]^{\mathrm{T}}\boldsymbol{B}_{1F}^{*},$$

$\bar{\boldsymbol{M}}_{1d}^{*}$ and $\bar{\boldsymbol{K}}_{1d}^{*}$ are the residual mass and stiffness matrices, respectively.

Equation (12) is the modal equation of Substructure 1 and is used for modal synthesis of the system. According to the same treatment for Substructures 2 and 3, two modal equations as Eq. (12) can be obtained and the processing procedure is omitted herein. Assembling the three modal equations yields

$$\bar{\boldsymbol{M}}^{*}\ddot{\bar{\boldsymbol{p}}} + \bar{\boldsymbol{K}}^{*}\bar{\boldsymbol{p}} = \bar{\boldsymbol{f}}^{*} + \bar{\boldsymbol{B}}^{*}\boldsymbol{F}, \tag{13}$$

where

$$\bar{\boldsymbol{p}} = [\bar{\boldsymbol{p}}_{1}^{\mathrm{T}} \ \ \bar{\boldsymbol{p}}_{2}^{\mathrm{T}} \ \ \bar{\boldsymbol{p}}_{3}^{\mathrm{T}}]^{\mathrm{T}}, \quad \bar{\boldsymbol{M}}^{*} = \mathrm{diag}(\bar{\boldsymbol{M}}_{1}^{*}, \ \bar{\boldsymbol{M}}_{2}^{*}, \ \bar{\boldsymbol{M}}_{3}^{*}),$$
$$\bar{\boldsymbol{K}}^{*} = \mathrm{diag}(\bar{\boldsymbol{K}}_{1}^{*}, \ \bar{\boldsymbol{K}}_{2}^{*}, \ \bar{\boldsymbol{K}}_{3}^{*}),$$
$$\bar{\boldsymbol{f}}^{*} = [(\bar{\boldsymbol{B}}_{1f}^{*}\boldsymbol{f}_{1\mathrm{J}})^{\mathrm{T}} \ \ (\bar{\boldsymbol{B}}_{2f}^{*}\boldsymbol{f}_{2\mathrm{J}})^{\mathrm{T}} \ \ (\bar{\boldsymbol{B}}_{3f}^{*}\boldsymbol{f}_{3\mathrm{J}})^{\mathrm{T}}]^{\mathrm{T}},$$
$$\bar{\boldsymbol{B}}^{*} = \begin{bmatrix}\bar{\boldsymbol{B}}_{1F}^{*} & \boldsymbol{0} & \boldsymbol{0} \\ \boldsymbol{0} & \bar{\boldsymbol{B}}_{2F}^{*} & \boldsymbol{0} \\ \boldsymbol{0} & \boldsymbol{0} & \bar{\boldsymbol{B}}_{3F}^{*}\end{bmatrix}, \quad \boldsymbol{F} = [F_{1} \ \ F_{2} \ \ F_{3}]^{\mathrm{T}}.$$

Equation (13) is not an independent coordinate equation of the system since the elements of $\bar{\boldsymbol{p}}$ are not independent. The vectors $\bar{\boldsymbol{p}}_1$, $\bar{\boldsymbol{p}}_2$ and $\bar{\boldsymbol{p}}_3$ all contain the interface DoFs of the system. Below we apply the displacement and force compatibility conditions of the three substructures to the removal of the redundant DoFs so as to obtain the independent coordinate equation of the system.

The displacement compatibility equation of the three substructures is

$$\boldsymbol{u}_{1\mathrm{J}} = \boldsymbol{u}_{2\mathrm{J}} = \boldsymbol{u}_{3\mathrm{J}}, \tag{14}$$

where $\boldsymbol{u}_{1\mathrm{J}}$, $\boldsymbol{u}_{2\mathrm{J}}$ and $\boldsymbol{u}_{3\mathrm{J}}$ are the vectors of interface coordinates of the three substructures, respectively. They can also be written as

$$\boldsymbol{u}_{1\mathrm{J}} = \boldsymbol{B}_{1}\boldsymbol{u}_{1}^{*}, \quad \boldsymbol{u}_{2\mathrm{J}} = \boldsymbol{B}_{2}\boldsymbol{u}_{2}^{*}, \quad \boldsymbol{u}_{3\mathrm{J}} = \boldsymbol{B}_{3}\boldsymbol{u}_{3}^{*}, \tag{15}$$

where $\boldsymbol{B}_1$, $\boldsymbol{B}_2$ and $\boldsymbol{B}_3$ are the Boolean indicated matrices of the three substructures, respectively, and their functions are to get the interface displacement vectors $\boldsymbol{u}_{1\mathrm{J}}$, $\boldsymbol{u}_{2\mathrm{J}}$ and $\boldsymbol{u}_{3\mathrm{J}}$ from the entire displacement vectors $\boldsymbol{u}_{1}^{*}$, $\boldsymbol{u}_{2}^{*}$ and $\boldsymbol{u}_{3}^{*}$. From Eq. (11), one can obtain

$$\boldsymbol{B}_{1}(\boldsymbol{\Phi}_{1k}\boldsymbol{p}_{1k} + \boldsymbol{\Psi}_{1d}\boldsymbol{f}_{1\mathrm{J}}) = \boldsymbol{B}_{2}(\boldsymbol{\Phi}_{2k}\boldsymbol{p}_{2k} + \boldsymbol{\Psi}_{2d}\boldsymbol{f}_{2\mathrm{J}}), \tag{16}$$
$$\boldsymbol{B}_{3}(\boldsymbol{\Phi}_{3k}\boldsymbol{p}_{3k} + \boldsymbol{\Psi}_{3d}\boldsymbol{f}_{3\mathrm{J}}) = \boldsymbol{B}_{2}(\boldsymbol{\Phi}_{2k}\boldsymbol{p}_{2k} + \boldsymbol{\Psi}_{2d}\boldsymbol{f}_{2\mathrm{J}}), \tag{17}$$

where $\boldsymbol{f}_{1\mathrm{J}}$, $\boldsymbol{f}_{2\mathrm{J}}$ and $\boldsymbol{f}_{3\mathrm{J}}$ are the interface-force vectors of the three substructures, respectively. Equations (16) and (17) are the compatibility equations of interface displacement described by the modal coordinate $\boldsymbol{p}_{ik}$ ($i = 1, 2, 3$) and the interface force $\boldsymbol{f}_{i\mathrm{J}}$ ($i = 1, 2, 3$). Based on Eqs. (16) and (17), $\boldsymbol{f}_{i\mathrm{J}}$ can be written as a function of $\boldsymbol{p}_{ik}$; thus it may be eliminated in the process of modal synthesis. The detailed process is given as follows.

From Eqs. (16) and (17), one can obtain

$$\begin{aligned}\boldsymbol{f}_{1\mathrm{J}} =& (\boldsymbol{B}_{1}\boldsymbol{\Psi}_{1d})^{-1}[\boldsymbol{B}_{2}(\boldsymbol{\Phi}_{2k}\boldsymbol{p}_{2k} + \\ & \boldsymbol{\Psi}_{2d}\boldsymbol{f}_{2\mathrm{J}}) - \boldsymbol{B}_{1}\boldsymbol{\Phi}_{1k}\boldsymbol{p}_{1k}],\end{aligned} \tag{18}$$

$$\begin{aligned}\boldsymbol{f}_{3\mathrm{J}} =& (\boldsymbol{B}_{3}\boldsymbol{\Psi}_{3d})^{-1}[\boldsymbol{B}_{2}(\boldsymbol{\Phi}_{2k}\boldsymbol{p}_{2k} + \\ & \boldsymbol{\Psi}_{2d}\boldsymbol{f}_{2\mathrm{J}}) - \boldsymbol{B}_{3}\boldsymbol{\Phi}_{3k}\boldsymbol{p}_{3k}].\end{aligned} \tag{19}$$

The condition of interface force of the three substructures is

$$\boldsymbol{f}_{1\mathrm{J}} + \boldsymbol{f}_{2\mathrm{J}} + \boldsymbol{f}_{3\mathrm{J}} = \boldsymbol{0}. \tag{20}$$

Substituting Eqs. (18) and (19) into Eq. (20) yields

$$\boldsymbol{f}_{2\mathrm{J}} = \boldsymbol{\Delta}_2[\boldsymbol{p}_{1k}\ \boldsymbol{p}_{2k}\ \boldsymbol{p}_{3k}]^{\mathrm{T}}, \tag{21}$$

where

$$\boldsymbol{\Delta}_2 = \boldsymbol{\Pi}_2^{-1}\begin{bmatrix} (\boldsymbol{B}_1\boldsymbol{\Psi}_{1d})^{-1}\boldsymbol{B}_1\boldsymbol{\Phi}_{1k} \\ -(\boldsymbol{B}_1\boldsymbol{\Psi}_{1d})^{-1}\boldsymbol{B}_2\boldsymbol{\Phi}_{2k}-(\boldsymbol{B}_3\boldsymbol{\Psi}_{3d})^{-1}\boldsymbol{B}_2\boldsymbol{\Phi}_{2k} \\ (\boldsymbol{B}_3\boldsymbol{\Psi}_{3d})^{-1}\boldsymbol{B}_3\boldsymbol{\Phi}_{3k} \end{bmatrix}^{\mathrm{T}},$$

$$\boldsymbol{\Pi}_2 = (\boldsymbol{B}_1\boldsymbol{\Psi}_{1d})^{-1}\boldsymbol{B}_2\boldsymbol{\Psi}_{2d} + \boldsymbol{I} + (\boldsymbol{B}_3\boldsymbol{\Psi}_{3d})^{-1}\boldsymbol{B}_2\boldsymbol{\Psi}_{2d}.$$

Substituting Eq. (21) into Eqs. (18) and (19) yields

$$\boldsymbol{f}_{1\mathrm{J}} = \boldsymbol{\Delta}_1\begin{bmatrix}\boldsymbol{p}_{1k}\\ \boldsymbol{p}_{2k}\\ \boldsymbol{p}_{3k}\end{bmatrix}, \quad \boldsymbol{f}_{3\mathrm{J}} = \boldsymbol{\Delta}_3\begin{bmatrix}\boldsymbol{p}_{1k}\\ \boldsymbol{p}_{2k}\\ \boldsymbol{p}_{3k}\end{bmatrix}, \tag{22}$$

where

$$\boldsymbol{\Delta}_1 = [-(\boldsymbol{B}_1\boldsymbol{\Psi}_{1d})^{-1}\boldsymbol{B}_1\boldsymbol{\Phi}_{1k}\ \ (\boldsymbol{B}_1\boldsymbol{\Psi}_{1d})^{-1}\boldsymbol{B}_2\boldsymbol{\Phi}_{2k}\ \ \boldsymbol{0}] + (\boldsymbol{B}_1\boldsymbol{\Psi}_{1d})^{-1}\boldsymbol{B}_2\boldsymbol{\Psi}_{2d}\boldsymbol{\Delta}_2,$$

$$\boldsymbol{\Delta}_3 = [\boldsymbol{0}\ \ (\boldsymbol{B}_3\boldsymbol{\Psi}_{3d})^{-1}\boldsymbol{B}_2\boldsymbol{\Phi}_{2k}\ \ -(\boldsymbol{B}_3\boldsymbol{\Psi}_{3d})^{-1}\boldsymbol{B}_3\boldsymbol{\Phi}_{3k}] + (\boldsymbol{B}_3\boldsymbol{\Psi}_{3d})^{-1}\boldsymbol{B}_2\boldsymbol{\Psi}_{2d}\boldsymbol{\Delta}_2.$$

The independent coordinate of the system is defined as

$$\boldsymbol{q} = [\boldsymbol{p}_{1k}\ \boldsymbol{p}_{2k}\ \boldsymbol{p}_{3k}]^{\mathrm{T}}. \tag{23}$$

The relationship between $\boldsymbol{q}$ and $\bar{\boldsymbol{p}}$ in Eq. (13) is

$$\bar{\boldsymbol{p}} = \begin{bmatrix}\boldsymbol{p}_{1k}\\ \boldsymbol{f}_{1\mathrm{J}}\\ \boldsymbol{p}_{2k}\\ \boldsymbol{f}_{2\mathrm{J}}\\ \boldsymbol{p}_{3k}\\ \boldsymbol{f}_{3\mathrm{J}}\end{bmatrix} = \boldsymbol{S}\boldsymbol{q} = \boldsymbol{S}\begin{bmatrix}\boldsymbol{p}_{1k}\\ \boldsymbol{p}_{2k}\\ \boldsymbol{p}_{3k}\end{bmatrix}, \tag{24}$$

where $\boldsymbol{S}$ is the coordinate transformation matrix that can be obtained by the matrix assembly of Eqs. (21) and (22). Substituting Eq. (24) into Eq. (13) and left multiplying $\boldsymbol{S}^{\mathrm{T}}$, one can obtain

$$\boldsymbol{M}\ddot{\boldsymbol{q}} + \boldsymbol{K}\boldsymbol{q} = \bar{\boldsymbol{B}}\boldsymbol{F}, \tag{25}$$

where

$$\boldsymbol{M} = \boldsymbol{S}^{\mathrm{T}}\bar{\boldsymbol{M}}^*\boldsymbol{S}, \quad \boldsymbol{K} = \boldsymbol{S}^{\mathrm{T}}\bar{\boldsymbol{K}}^*\boldsymbol{S}, \quad \bar{\boldsymbol{B}} = \boldsymbol{S}^{\mathrm{T}}\bar{\boldsymbol{B}}^*.$$

Since the interface force appears in pairs in the structural system, only the external force $\boldsymbol{F}$ appears in the right hand of Eq. (25). Equation (25) is the final dynamic equation of the system obtained by the double-compatible modal synthesis method, and can be used for dynamic analysis and control design for the system. In this equation, all the interface forces are eliminated and only the low-order modal coordinates of each component of the system are preserved, so the order dimension of Eq. (25) is the amount sum of the preserved low-order modes of all components of the system.

1.2 Numerical Simulations

Numerical simulations are carried out to demonstrate the validity of the proposed modeling method in this paper. In Fig. 2, the length of long beam is $l_2 = 55\,\mathrm{m}$, the cross section area is $A_2 = 1.217\,7\,\mathrm{m}^2$, the elasticity modulus is $E_2 = 72\,\mathrm{GPa}$ and the mass is $m_2 = 1.815\,0\times 10^5\,\mathrm{kg}$. The corresponding parameters of the two short beams are: $l_1 = l_3 = 15\,\mathrm{m}$, $A_1 = A_3 = 0.545\,4\,\mathrm{m}^2$, $E_1 = E_3 = 72\,\mathrm{GPa}$ and $m_1 = m_3 = 2.217\,1\times 10^4\,\mathrm{kg}$.

In the FEM, the long beam is divided into 55 elements and the short beam is divided into 15 elements, so there are 56 nodes and 168 DoFs for the long beam, and 16 nodes and 48 DoFs for the short beam. The total number of DoFs of the system is 264. In the modal truncation method for the three substructures, the top 1/3 modes of the long beam and the first ten modes of the two short beams are preserved, so the total number of the preserved modes of the system is 76. Therefore, the order of the reduction model established by the double-compatible modal synthesis method is 76. We can see that the model order of the system has been reduced greatly. Natural frequencies of the system obtained by the FEM and the double-compatible modal synthesis method are compared numerically to verify the validity of the reduction model. Table 1 shows the results of the first thirty frequencies. The results obtained by the FEM and the double-compatible modal synthesis method are compared with the results obtained by the classical free-interface and fixed-interface modal synthesis methods. The first three frequencies in Table 1 are zero, representing the rigid modes of the system. Here we display the frequency error using the frequency ratio ω'/ω_0, where ω_0 represents the natural frequency obtained by the FEM, and ω' represents the natural frequency obtained by the free-interface, fixed-interface and double-compatible modal synthesis methods, separately. The frequency error is shown in Fig. 3, and Fig. 3(b) is the enlarged figure of Fig. 3(a). We can observe from Table 1 and Fig. 3 that the results of the double-compatible modal synthesis method agree well with those of the FEM. The free-interface modal synthesis method is superior to the fixed-interface modal synthesis method, but they are both worse than the double-compatible modal synthesis method. The low-order frequencies of the free-interface and fixed-interface modal synthesis methods show agreement with those of the FEM and the double-compatible modal synthesis method, but big error appears in high-order frequency band. The computational precision of the double-compatible modal synthesis method is obviously higher than that of the classical free-interface and fixed-interface modal synthesis methods.

The frequency response of flexible vibration of the system is also used as the judgment standard to evaluate the effectiveness of dynamic model. Two models

Table 1 The first thirty natural frequencies of the system

Order of mode	Natural frequency/Hz			
	FEM	Free-interface method	Fixed-interface method	Double-compatible method
1	0	0	0	0
2	0	0	0	0
3	0	0	0	0
4	6.257 547 462	6.257 560 888	6.260 776 584	6.257 547 462
5	16.995 141 24	16.995 357 97	17.006 187 90	16.995 141 24
6	33.704 997 31	33.705 959 91	33.730 669 42	33.704 997 31
7	35.878 142 97	35.895 658 42	35.896 631 54	35.878 143 00
8	40.896 853 57	40.911 225 85	40.922 389 48	40.896 853 61
9	42.066 112 51	42.134 099 80	42.237 862 73	42.066 112 61
10	57.063 759 05	57.065 304 68	57.113 534 44	57.063 759 05
11	83.513 103 03	83.516 416 81	83.782 258 89	83.513 103 19
12	93.996 676 82	94.205 676 40	94.500 476 29	93.996 684 78
13	111.803 043 0	111.822 581 4	112.548 500 3	111.803 045 9
14	133.901 926 6	134.041 344 0	134.035 672 3	133.901 942 3
15	139.600 309 2	139.681 124 4	139.961 115 8	139.600 321 6
16	144.658 093 0	144.788 824 5	146.173 336 9	144.658 123 1
17	147.534 033 2	147.553 245 6	149.497 131 5	147.534 042 7
18	184.752 247 5	184.797 023 1	196.789 700 2	184.752 281 6
19	187.189 099 9	187.199 463 7	198.831 292 2	187.189 112 9
20	198.730 493 2	206.883 626 1	243.794 099 9	198.740 741 1
21	198.730 493 2	209.934 096 6	252.929 930 2	198.745 027 1
22	225.519 212 7	225.568 983 0	272.768 181 6	225.519 274 6
23	229.716 080 9	230.366 634 1	275.301 476 3	229.716 885 1
24	263.947 316 3	264.113 922 9	393.152 971 3	263.947 945 9
25	271.585 856 9	271.785 291 6	400.568 208 5	271.587 302 1
26	274.350 262 0	274.409 230 3	432.236 550 7	274.350 696 2
27	283.209 025 6	283.881 022 7	432.237 746 4	283.211 419 3
28	311.256 124 9	311.352 991 2	450.723 827 4	311.256 785 6
29	332.662 458 7	332.774 649 5	597.085 542 4	332.663 355 1
30	359.927 785 8	359.932 532 1	600.044 711 8	359.927 845 5

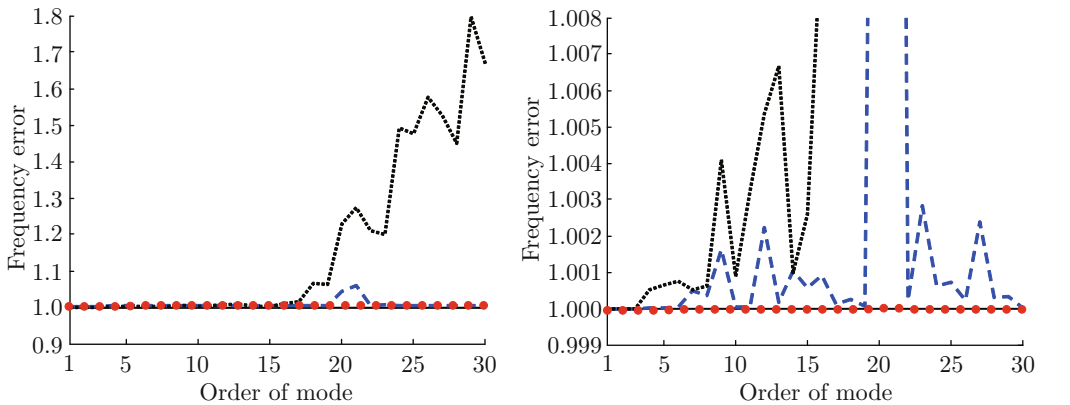

(a) Complete graph (b) Partial enlarged graph

Fig. 3 Frequency error of the system

are used in the simulations: ① the FEM model of the system; ② the reduction model with 76 DoFs obtained by the double-compatible modal synthesis method. The simulation results are shown in Fig. 4. The result using the reduction model agrees better with that using the FEM model. The reduction model can reflect the dynamic characteristics of the original system effectively.

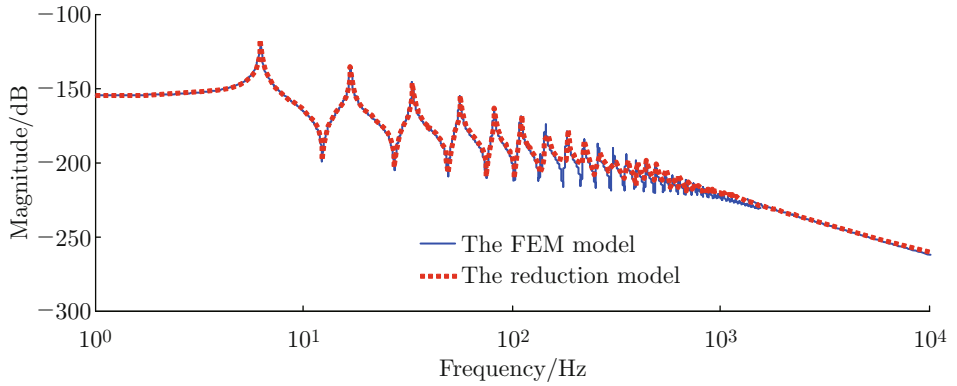

Fig. 4 Frequency response using the FEM model and the model of modal synthesis method

2 Active Control Design

In this section, control design problem is studied. The flight trajectory of the launch vehicle is firstly introduced, then a control law for the system is designed by using the swing angle of rocket thrust as design variable, sequentially the calculation method for the deflection of mass center of the launch vehicle is given, and finally numerical simulation is done to verify the validity of the control law.

2.1 Brief Introduction to Trajectory of Launch Vehicle

The high earth orbit and the low earth orbit are two different flight phases of strap-on launch vehicle from ignition and lift-off to launching satellite into the desired spatial position. The space conditions of the launch vehicle in the two phases are different, so the demand of dynamic analysis for the vehicle is different too. In the low earth orbit, the launch vehicle is put into orbit by the stage engines burning continuously one after another so that the required orbital velocity is achieved at the end of the powered phase of the trajectory, so this phase is called the active flight one. The gravity variation along with the flight height of the launch vehicle in this phase may be neglected since the flight height in this phase is very smaller than the earth radius. The horizontal distance of flight of the launch vehicle in this phase is small too. The influence of the earth curvature is so little that it can be neglected. When the launch vehicle reaches to the position of the height of 130 km and the horizontal distance of 160 km, the rocket engine burns out and the launch vehicle begins to fly under its inertia, so this phase may be called the unpowered flight one or the free flight one. When the launch vehicle is close to the desired satellite orbit, the rocket engine ignites again to develop a thrust to accelerate the launch vehicle to the required speed and the desired satellite orbit. Figure 5 shows the three flight phases of the launch vehicle mentioned above. In this paper, we consider an active control problem of the vehicle in the active flight phase.

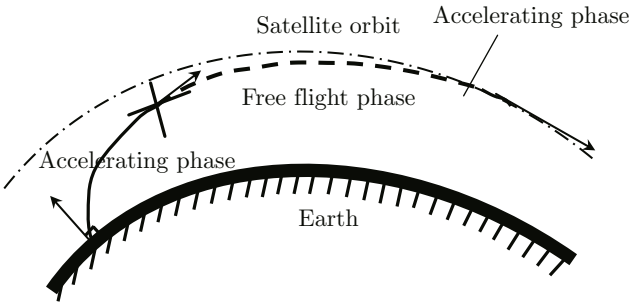

Fig. 5 Schematic diagram of trajectory of launch vehicle

2.2 Control Law Design

When the launch vehicle is regarded as a mass point, the force analysis is illustrated in Fig. 6, where mg is the gravity and F is the total thrust. From Figs. 1 and 2, we know that $F = F_1 + F_2 + F_3$ and $m = m_1 + m_2 + m_3$. In Fig. 6, v is the flight velocity of the launch vehicle, θ is the angle between the thrust and the horizontal direction, and γ is the angle between the flight velocity and the horizontal direction. For simplicity, the mass of the launch vehicle is assumed to be constant during the flight. The motion equation of the vehicle can be

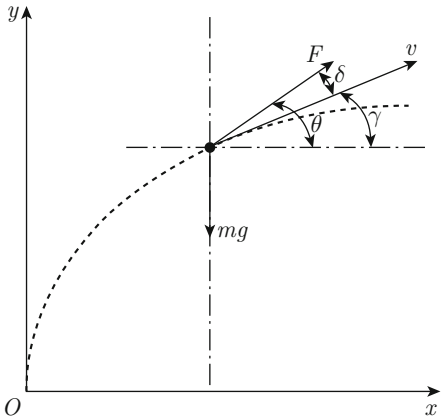

Fig. 6 Schematic diagram of force and motion

written as

$$\left.\begin{aligned} m\ddot{x} &= F\cos\theta \\ m\ddot{y} &= F\sin\theta - mg \end{aligned}\right\}. \tag{26}$$

The launch vehicle remains vertical before launch. The thrust direction is vertical too in the beginning of rocket launch. Then it is changed to make the vehicle travel with the pre-designed trajectory. From Ref. [24] we know that the thrust value of a launch vehicle is generally constant and the angle δ between the thrust and flight velocity direction is often used as the design variable of control. According to Ref. [24], we design δ.

It is pointed out in Ref. [24] that the total time of active flight phase for a typical flight of launch vehicle is about 160 s, where the vertical ascent is from 0 to 7 s, namely $\theta = 90°$ at $t \in [0, 7]$ s; in the period of $[7, 87]$ s, θ changes uniformly from 90° to 30°, and θ keeps 30° in the period of $[87, 160]$ s. The change law of θ is shown in Fig. 7. When the thrust F is known, the horizontal and vertical flight distances, x and y, the flight speed v and the angle γ can be obtained by Eq. (26). So the control law δ can be computed by $\delta = \theta - \gamma$. The deflection of mass center of the system can be calculated by applying this control law to the flexible vibration model of the launch vehicle.

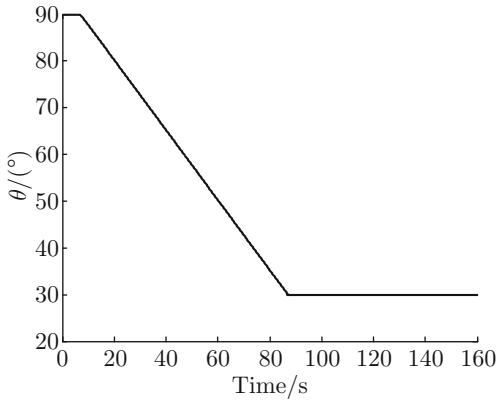

Fig. 7 Time history of θ given in Ref. [24]

2.3 Deflection of Mass Center of the Launch Vehicle

In this paper, the deflection of mass center of the launch vehicle is calculated numerically. It is expected that this deflection should be as small as possible during the flight of the launch vehicle. The dynamic equation of the launch vehicle system established by the modal synthesis method is shown in Eq. (25). The launch vehicle system is a positive semi-definite system. Equation (25) contains three DoFs of the rigid body, namely the rigid body motions of the system in the axial, transverse and rotational directions, respectively. Since the launch vehicle is essentially a long slender beam, the axial and rotational deflections of mass center are much smaller than the transverse one, so we only consider the transverse deflection in the simulation. The launch vehicle is a symmetric structure as shown in Fig. 1, and the mass centre is located in the core stage. From Fig. 8, the position of mass centre of the system can be written as

$$y_0 = \frac{m_1 y_1 + m_2 y_2 + m_3 y_3}{m_1 + m_2 + m_3}, \tag{27}$$

where y_1, y_2 and y_3 are the mass centre coordinates of the three substructures, respectively.

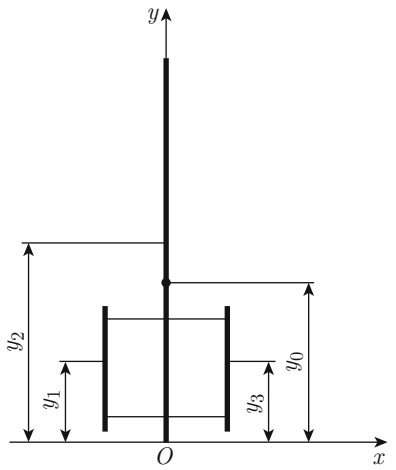

Fig. 8 Position of mass center of the system

In order to calculate the deflection of mass center by Eq. (25), the three DoFs of rigid body should be removed from this equation to obtain the flexible vibration equation of the system. Next we introduce a method to obtain the flexible vibration equation.

Equation (25) may be divided into the rigid body motion and the flexible body motion by

$$\boldsymbol{q} = \boldsymbol{q}_{\mathrm{g}} + \boldsymbol{q}_{\mathrm{e}} = \boldsymbol{T}_{\mathrm{g}}\boldsymbol{\eta}_{\mathrm{g}} + \boldsymbol{T}_{\mathrm{e}}\boldsymbol{\eta}_{\mathrm{e}}, \tag{28}$$

where $\boldsymbol{q}_{\mathrm{g}}$ and $\boldsymbol{q}_{\mathrm{e}}$ are the displacement vectors of rigid and flexible body motions of the system, respectively; $\boldsymbol{T}_{\mathrm{g}}$ and $\boldsymbol{T}_{\mathrm{e}}$ are the corresponding modal matrices, and $\boldsymbol{\eta}_{\mathrm{g}}$ and $\boldsymbol{\eta}_{\mathrm{e}}$ are the corresponding modal coordinates. Since there exist only three rigid modes in the system, $\boldsymbol{T}_{\mathrm{g}}$ can be written as $\boldsymbol{T}_{\mathrm{g}} = [\boldsymbol{T}_{\mathrm{g1}}\ \ \boldsymbol{T}_{\mathrm{g2}}\ \ \boldsymbol{T}_{\mathrm{g3}}]$, where $\boldsymbol{T}_{\mathrm{g1}}$, $\boldsymbol{T}_{\mathrm{g2}}$ and $\boldsymbol{T}_{\mathrm{g3}}$ are the rigid modes in the axial, transverse and rotational directions, respectively.

Substituting Eq. (28) into Eq. (25), one can obtain the flexible vibration equation:

$$\boldsymbol{M}\ddot{\boldsymbol{q}}_{\mathrm{e}} + \boldsymbol{K}\boldsymbol{q}_{\mathrm{e}} = \bar{\boldsymbol{B}}\boldsymbol{F} - \boldsymbol{M}\boldsymbol{T}_{\mathrm{g}}\ddot{\boldsymbol{\eta}}_{\mathrm{g}}. \tag{29}$$

From the theory of modal orthogonality, we know that $\boldsymbol{T}_{\mathrm{g}}$ and $\boldsymbol{T}_{\mathrm{e}}$ are mass-orthogonal and stiffness-orthogonal, so $\boldsymbol{T}_{\mathrm{g}}^{\mathrm{T}}\boldsymbol{M}\boldsymbol{T}_{\mathrm{e}} = \boldsymbol{0}$ and $\boldsymbol{T}_{\mathrm{g}}^{\mathrm{T}}\boldsymbol{K}\boldsymbol{T}_{\mathrm{e}} = \boldsymbol{0}$. Multiplying $\boldsymbol{T}_{\mathrm{g}}^{\mathrm{T}}$ for Eq. (29) yields

$$\boldsymbol{T}_{\mathrm{g}}^{\mathrm{T}}\bar{\boldsymbol{B}}\boldsymbol{F} - \boldsymbol{T}_{\mathrm{g}}^{\mathrm{T}}\boldsymbol{M}\boldsymbol{T}_{\mathrm{g}}\ddot{\boldsymbol{\eta}}_{\mathrm{g}} = \boldsymbol{0}. \tag{30}$$

When $\boldsymbol{T}_{\mathrm{g}}$ is the normalized mode, there is $\boldsymbol{T}_{\mathrm{g}}^{\mathrm{T}}\boldsymbol{M}\boldsymbol{T}_{\mathrm{g}} = \boldsymbol{I}$, so Eq. (30) can be written as

$$\ddot{\boldsymbol{\eta}}_{\mathrm{g}} = \boldsymbol{T}_{\mathrm{g}}^{\mathrm{T}}\bar{\boldsymbol{B}}\boldsymbol{F}. \tag{31}$$

Substituting Eq. (31) into Eq. (29) yields

$$\boldsymbol{M}\ddot{\boldsymbol{q}}_{\mathrm{e}} + \boldsymbol{K}\boldsymbol{q}_{\mathrm{e}} = \bar{\boldsymbol{B}}\boldsymbol{F} - \boldsymbol{M}\boldsymbol{T}_{\mathrm{g}}\boldsymbol{T}_{\mathrm{g}}^{\mathrm{T}}\bar{\boldsymbol{B}}\boldsymbol{F} = \boldsymbol{B}\bar{\boldsymbol{B}}\boldsymbol{F}, \tag{32}$$

where $\boldsymbol{B} = \boldsymbol{I}_{\mathrm{g}} - \boldsymbol{M}\boldsymbol{T}_{\mathrm{g}}\boldsymbol{T}_{\mathrm{g}}^{\mathrm{T}}$. Equation (32) is the flexible vibration equation of the system that the rigid body motion is removed.

2.4 Numerical Simulations

Control simulations are carried out in this section. The parameters of the launch vehicle are the same as those in Subsection 1.2. According to Ref. [24], the thrust of the core stage is chosen as $F_2 = 2.961\,6$ MN and those of the two boosters are $F_1 = F_3 = 1.484\,\mathrm{MN}$, so the total thrust is $F = 5.929\,6\,\mathrm{MN}$. The arrangement of flight time of the launch vehicle given in Ref. [24] is used herein, and can be found in Subsection 2.2 too. The change law of θ is shown in Fig. 7. The mass centre position is determined to be $y_0 = 23.57\,\mathrm{m}$.

Figure 9(a) shows the time history of the angle γ between the vehicle velocity and the horizontal direction. Figure 9(b) shows the changing curve of the angle δ between the directions of the thrust and the vehicle velocity. Figure 10 displays the deflection of mass centre of the system in the transverse direction. Figure 10(b) is the enlarged figure of Fig. 10(a) in $[120, 130]\,\mathrm{s}$. It is observed from Fig. 10(b) that the mass center behaves with a very small vibration near its equilibrium position. Figure 11 illustrates the change of the horizontal and vertical distances of the launch vehicle.

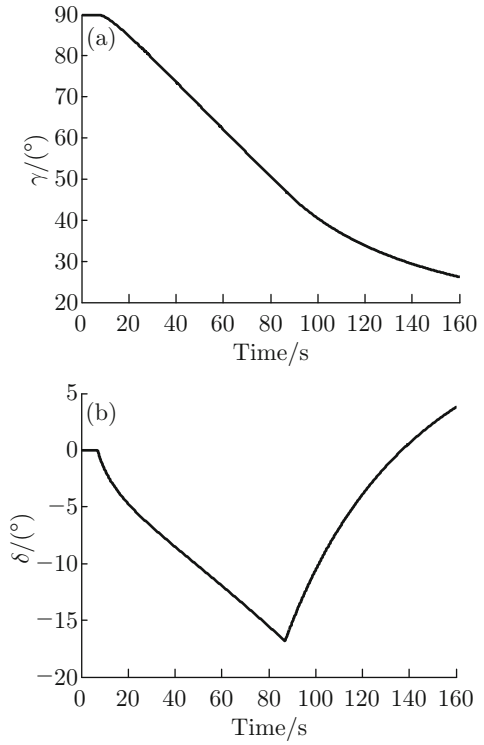

Fig. 9 Time history of the angle γ and δ

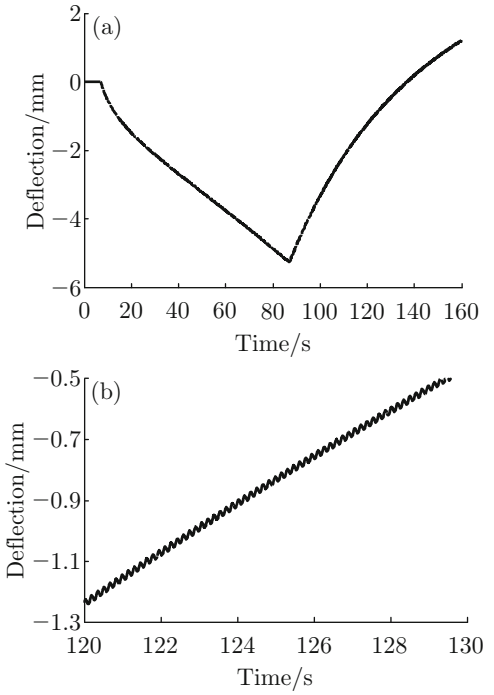

Fig. 10 Deflection of mass centre of the system

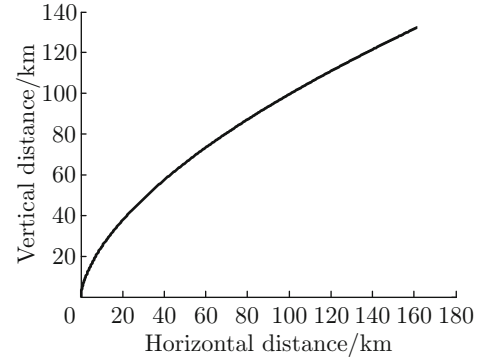

Fig. 11 Change of horizontal and vertical distances

3 Conclusion

In this paper, dynamic modeling and active control of a strap-on launch vehicle are studied. The double-compatible modal synthesis method is used to establish the dynamic model of the system, and the control law design based on the model of mass center motion is applied to the system to verify its validity. The computational precision of the double-compatible modal synthesis method is numerically compared with that of the classical free-interface and fixed-interface modal synthesis methods. Simulation results indicate that

the computational precision of the double-compatible modal synthesis method is much higher than that of the free-interface and fixed-interface modal synthesis methods. The dynamic model established by the double-compatible modal synthesis method is effective in describing the dynamic characteristics of the original system. The mass center of the launch vehicle behaves with a very small vibration near its equilibrium position under the action of the given control law.

References

[1] MORGAN J A. Dynamic analysis of coupled substructures using experimentally-based component mode synthesis [D]. Ann Arbor MI, USA: Mechanical Engineering, The University of Michigan, 1996.

[2] CRAIG R R, CHANG C J. Substructure coupling for dynamic analysis and testing [M]. Washington, USA: Press of National Aeronautics and Space Administration, 1977.

[3] WANG Y Y. Dynamic substructure method theory and applications [M]. Beijing, China: Science Press, 1999 (in Chinese).

[4] WANG W L, DU Z R. Study of vibration and dynamic substructure technique [M]. Shanghai, China: Fudan University Press, 1985 (in Chinese).

[5] WU X S, WANG W L. A double compatible dynamic substructure technique for aircraft structural borne interior noise analysis [J]. *Acta Mechanica Sinica*, 1987, **19**(Sup): 127-131 (in Chinese).

[6] BLADH R, CASTANIER M P, PIERRE C. Component-mode-based reduced order modeling techniques for mistuned bladed disks. Part I. Theoretical models [J]. *Journal of Engineering for Gas Turbines and Power*, 2001, **123**(1): 89-99.

[7] BLADH R, CASTANIER M P, PIERRE C. Component-mode-based reduced order modeling techniques for mistuned bladed disks. Part II. Application [J]. *Journal of Engineering for Gas Turbines and Power*, 2001, **123**(1): 100-108.

[8] CASTANIER M P, TAN Y C, PIERRE C. Characteristic constraint modes for component mode synthesis [J]. *AIAA Journal*, 2001, **39**(6): 1182-1187.

[9] KARPEL M, MOULIN B, FELDGUN V. Component mode synthesis of a vehicle system model using the fictitious mass method [J]. *Journal of Vibration and Acoustics*, 2007, **129**(1): 73-83.

[10] PAPADIMITRIOU C, PAPADIOTI D C. Component mode synthesis techniques for finite element model updating [J]. *Computers and Structures*, 2013, **126**: 15-28.

[11] BLADH J R. Efficient predictions of the vibratory response of mistuned bladed disks by reduced order modeling [D]. Ann Arbor MI, USA: Mechanical Engineering, The University of Michigan, 2001.

[12] QIN Z Y, YAN S Z, CHU F L. Dynamic characteristics of launch vehicle and spacecraft connected by clamp band [J]. *Journal of Sound and Vibration*, 2011, **330**(10): 2161-2173.

[13] LI J L, YAN S Z, TAN X F. Dynamic-envelope analysis of clamp-band joint considering pyroshock of satellite separation [J]. *Journal of Spacecraft and Rockets*, 2014, **51**(5), 1390-1400.

[14] TEWARI A. Advanced control of aircraft, spacecraft and rockets [M]. New York, USA: John Wiley & Sons, 2011.

[15] WIE B. Space vehicle dynamics and control [M]. Reston, USA: Press of American Institute of Aeronautics and Astronautics, 2008.

[16] HUGHES P C. Spacecraft attitude dynamics [M]. New York, USA: John Wiley & Sons, 1986.

[17] WERTZ J R. Spacecraft attitude determination and control [M]. Boston, USA: Kluwer Academic Publishers, 1978.

[18] KAPLAN M H. Modern spacecraft dynamics and control [M]. New York, USA: John Wiley & Sons, 1976.

[19] LANDON V, STEWART B. Notational stability of an axisymmetric body containing a rotor [J]. *Journal of Spacecraft and Rockets*, 1964, **1**(6): 682-684.

[20] LIKINS P W. Attitude stability for dual-spin spacecraft [J]. *Journal of Spacecraft and Rockets*, 1967, **4**(12): 1638-1643.

[21] OCONNOR B J, MORINE L A. A description of the CMG and its application to space vehicle control [J]. *Journal of Spacecraft and Rockets*, 1969, **6**(3): 225-231.

[22] WHORTON M S, HALL C E, COOK S A. Ascent flight control and structural interaction for the Ares-I crew launch vehicle [C]//*48th AIAA/ASME/ASCE/AHS/ASC Structures, Structural Dynamics and Materials Conference*. Honolulu, Hawaii: AIAA, 2007: 1780-1792.

[23] WEI D. Dynamic modeling and ascent flight control of Ares-I crew launch vehicle [D]. Ames, Iowa, USA: Aerospace Engineering, Iowa State University, 2000.

[24] QIAN X S. Introduction to the interstellar flight [M]. Beijing, China: China Astronautics Publishing House, 2008 (in Chinese).